BRAIN COMMUNICATIONS

Adenosine kinase inhibition promotes proliferation of neural stem cells after traumatic brain injury

Hoda M. Gebril,[1,2] **Rizelle Mae Rose,**[2] **Raey Gesese,**[2] **Martine P. Emond,**[2] **Yuqing Huo,**[3] **Eleonora Aronica**[4,5] **and** (iD)**Detlev Boison**[1]

Traumatic brain injury (TBI) is a major public health concern and remains a leading cause of disability and socio-economic burden. To date, there is no proven therapy that promotes brain repair following an injury to the brain. In this study, we explored the role of an isoform of adenosine kinase expressed in the cell nucleus (ADK-L) as a potential regulator of neural stem cell proliferation in the brain. The rationale for this hypothesis is based on coordinated expression changes of ADK-L during foetal and postnatal murine and human brain development indicating a role in the regulation of cell proliferation and plasticity in the brain. We first tested whether the genetic disruption of ADK-L would increase neural stem cell proliferation after TBI. Three days after TBI, modelled by a controlled cortical impact, transgenic mice, which lack ADK-L (ADK$^{\Delta neuron}$) in the dentate gyrus (DG) showed a significant increase in neural stem cell proliferation as evidenced by significant increases in doublecortin and Ki67-positive cells, whereas animals with transgenic overexpression of ADK-L in dorsal forebrain neurons (ADK-L^{tg}) showed an opposite effect of attenuated neural stem cell proliferation. Next, we translated those findings into a pharmacological approach to augment neural stem cell proliferation in the injured brain. Wild-type C57BL/6 mice were treated with the small molecule adenosine kinase inhibitor 5-iodotubercidin for 3 days after the induction of TBI. We demonstrate significantly enhanced neural stem cell proliferation in the DG of 5-iodotubercidin-treated mice compared to vehicle-treated injured animals. To rule out the possibility that blockade of ADK-L has any effects in non-injured animals, we quantified baseline neural stem cell proliferation in ADK$^{\Delta neuron}$ mice, which was not altered, whereas baseline neural stem cell proliferation in ADK-L^{tg} mice was enhanced. Together these findings demonstrate a novel function of ADK-L involved in the regulation of neural stem cell proliferation after TBI.

1 Department of Neurosurgery, Robert Wood Johnson Medical School, Rutgers University, Piscataway, NJ 08854, USA
2 Robert Stone Dow Neurobiology Laboratories, Legacy Research Institute, Portland, OR 97232, USA
3 Department of Cellular Biology & Anatomy, Medical College of Georgia, Vascular Biology Center, Augusta University, Augusta, GA 30912, USA
4 Department of (Neuro)Pathology, Academic Medical Center and Swammerdam Institute for Life Sciences, Center for Neuroscience, University of Amsterdam, Amsterdam, The Netherlands
5 Stichting Epilepsie Instellingen (SEIN) Nederland, Heemstede, The Netherlands

Correspondence to: Detlev Boison
Department of Neurosurgery, Robert Wood Johnson Medical School
Rutgers University, 683 Hoes Ln W, Piscataway, NJ 08854, USA.
E-mail: detlev.boison@rutgers.edu

Keywords: Traumatic brain injury; dentate gyrus; neurogenesis; regeneration; adenosine kinase

Abbreviations: ADK-L = adenosine kinase long; ADK-S = adenosine kinase short; BDNF = brain-derived neurotrophic factor; CCI = control cortical impactor; CP = cortical plate; DG = dentate gyrus; DCX = doublecortin; FGF-1 = fibroblast growth factor; 5-ITU = 5-iodotubercidin; GFAP = glial fibrillary acidic protein; GW = gestational week; IR = immunoreactivity; ROI = region of interest; SEM = standard error of mean; SVZ = subventricular zone; TBI = traumatic brain injury; VZ = ventricular zone; WT = wild type

Graphical Abstract
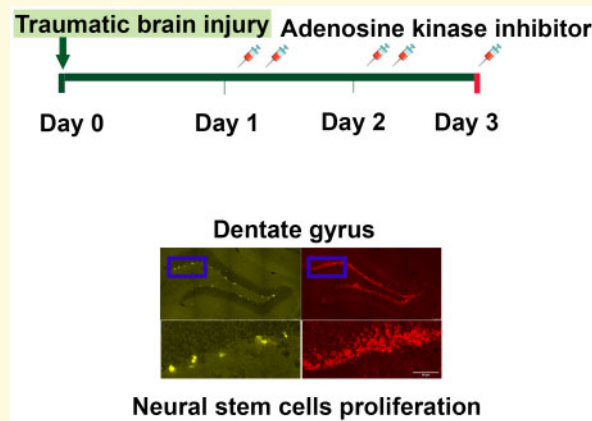
Introduction

Traumatic brain injury (TBI) is one of the leading causes of disability. Human rehabilitation studies suggest that the injured brain maintains a limited capacity for self-repair in line with studies showing that the adult brain is capable of generating new neurons, especially after brain injury (Altman and Das, 1965; Neuberger *et al.*, 2017). Understanding endogenous repair mechanisms holds promise for the development of novel regeneration-promoting therapies. Experimental models show that TBI is a potent trigger of neural stem cell proliferation (Dash *et al.*, 2001; Gao *et al.*, 2009); however, the mechanisms that contribute to post-injury neurogenesis are incompletely understood.

Adult neurogenesis is a highly regulated process where the molecular machinery is under the control of various internal and external cues (Goncalves *et al.*, 2016; Hsieh and Zhao, 2016). One of the contributing mechanisms is based on epigenetic modifications of genes crucial in controlling proliferation, differentiation and maturation of neural stem cells in the dentate gyrus (DG). Several lines of evidence demonstrate the involvement of epigenetic modifications in the regulation of genes encoding neurotrophic factors such as brain-derived neurotrophic factors (BDNF) and fibroblast growth factor-1 (FGF-1), which in turn affect self-renewal, plasticity, proliferation and differentiation of neural stem cells in the DG (Aid *et al.*, 2007; Ma *et al.*, 2009). Interestingly, further epigenetic modifications of the *BDNF* gene are associated with changes in the neurogenic niche after brain injury (Griesbach *et al.*, 2002; Gao *et al.*, 2006; Miao *et al.*, 2015). To date, the mechanisms orchestrating those epigenetic modifications are yet to be understood.

Adenosine kinase (ADK; EC 2.7.1.20) is the key regulator of intra- and extracellular adenosine levels in the brain (Boison, 2013). The enzyme exists in two isoforms, a short version (ADK-S; 38.7 kDa) expressed in the cytoplasm and a long version (ADK-L; 40.5 kDa) expressed in the nucleus. Both are derived from the same gene through alternative splicing and promoter use (Cui *et al.*, 2009). Whereas ADK-S controls extracellular levels of adenosine and hence adenosine receptor activation, which is important for the control of seizures (Huber *et al.*, 2002; Li *et al.*, 2009), ADK-L controls epigenetic functions, in particular DNA methylation (Boison, 2013). In this latter epigenetic role, adenosine controls the rate of DNA methylation via interference with the transmethylation pathway. DNA methylation changes in turn is one of the candidate mechanisms regulating brain development, maturation, plasticity, and cell proliferation (Costello et al., 2003; Hirabayashi et al., 2013). Therefore, adenosine is a candidate mechanism for the regulation of genes implicated in cell proliferation in the brain.

During brain development, ADK undergoes coordinated expression changes from neurons to astrocytes (Studer *et al.*, 2006), whereby in the adult brain ADK expression is limited to plastic cells with proliferative potential, such as astrocytes (Fedele *et al.*, 2004). In adult mice, ADK-L expression is maintained in nuclei of granular neurons of the DG, a neurogenic zone, suggesting an important role of ADK-L in cell proliferation in the brain. We therefore assessed whether ADK-L affects neural stem cell proliferation after TBI. We first assessed ADK-L expression within the context of developmental and proliferative processes in the human brain making use of foetal brain

specimens. We next demonstrated that the lack of ADK-L in dentate granular neurons of mice specifically enhanced neural stem cell proliferation after a TBI, but not in normal subjects, whereas an increase in ADK-L had the opposite effect. We finally validated those findings with a pharmacological approach to enhance neural stem cell proliferation after TBI. Together, our findings define ADK-L as a novel contributor to the regulation of acute neural stem cell proliferation after TBI.

Materials and methods

Human material

Foetal brain tissue was obtained from the repository of the Department of Neuropathology of the University Hospital Amsterdam. Informed consent was obtained for the use of brain tissue and for access to medical records for research purposes. Tissue was obtained and used in a manner compliant with the Declaration of Helsinki. The expression of ADK was evaluated at the following ages: 9, 13, 17, 20, 23, 25, 29, 31, 36 and 40 gestational weeks (GWs) obtained from spontaneous or medically induced abortions with appropriate maternal written consent for brain autopsy. All autopsies were performed within 12 h after death. Human tissue was fixed in 10% buffered formalin and embedded in paraffin. Paraffin-embedded tissue was sectioned at 6 μm, mounted on pre-coated glass slides (StarFrost, Waldemar Knittel Glasbearbeitungs GmbH, Braunschweig, Germany) and used for immunohistochemical staining as described below.

Antibody characterization

For the detection of human ADK, a polyclonal rabbit antibody was used as described in Studer et al. (2006), and according to Boison and Aronica (2015). We also used a commercial antibody (Bethyl Labs, A304-280A, 1:1000), which gave identical results. This latter antibody was previously validated in mice with an engineered deletion of ADK in the brain (Sandau et al., 2016). The antibody specificity in human tissue was further tested by Western blot analysis of the total homogenates of human control brain revealing a band of approximately 40 kDa (not shown), and compared with lack of ADK staining in Western Blots or on tissue from ADK knockout samples (Boison et al., 2002; Fedele et al., 2004; Gouder et al., 2004).

Immunohistochemistry of human tissue

For single-labeling, paraffin-embedded sections were deparaffinized, re-hydrated and incubated for 20 min in 0.3% H_2O_2 diluted in methanol to quench the endogenous peroxidase activity. Antigen retrieval was performed by incubation for 10 min at 121°C in citrate buffer (0.01 M, pH 6.0). Sections were washed with phosphate-buffered saline (PBS), and incubated for 30 min in 10% normal goat serum (Harlan Sera-Lab, Loughborough, Leicestershire, UK). After the primary antibodies incubated overnight at 44°C, the sections were washed in PBS and the ready-for-use Powervision peroxidase system was used (Immunologic, Duiven, The Netherlands) and 3,3'-diaminobenzidine (DAB; Sigma) as chromogen to visualize the antibodies. Sections were counterstained with haematoxylin, dehydrated and coverslipped. Sections incubated without the primary Ab or with pre-immune sera were essentially blank.

Transgenic mice

In vivo studies were conducted in an AAALAC accredited facility in accordance with approved Legacy IACUC protocols and under adherence to the ARRIVE guidelines. All mice were generated and propagated on an identical C57BL/6 background and were social-housed under standardized conditions of light, temperature and humidity, environmental enrichment and had access to food and water *ad libitum*. For this study, we used male mice aged 2–4 months. Experimental mice were generated by breeding Adk-flox mice ($Adk^{fl/fl}$) (Caplan et al., 2017) with CamKIIα-Cre mice (Schweizer et al., 2003) to generate CamKIIα-Cre$^{+/-}$:Adk$^{fl/fl}$ mice. Breeding of the experimental animals followed a CamKIIα-Cre$^{+/-}$:Adk$^{fl/fl}$ x Adk$^{fl/fl}$ mating protocol, which generated ADK$^{\Delta neuron}$ and normal Adk$^{fl/fl}$ mice in a 1:1 ratio as littermates. ADK-L^{tg} mice were produced using a transgene vector, in which the cDNA coding for the long isoform of ADK (Adk-L) was driven by the same $CamKIIα$-promoter described above. ADK-L^{tg} mice were maintained as a heterozygous line with ADK-L^{tg} and wild-type (WT) mice produced as littermates. Control mice used in this study included littermates from both lines (Adk$^{fl/fl}$ and Adk$^{+/+}$).

Controlled cortical impact

Both WT and transgenic mice were exposed to moderate-to-severe controlled cortical impact (CCI) injury in accordance with procedures previously reported (Romine et al., 2014). Briefly, mice (total $n = 28$, weight 23 ± 0.68 g) were anaesthetized using 3% isoflurane, then the heads were shaved and the animals were fixed in a stereotaxic frame (Kopf, Tujunga, CA). The animals were placed on a heating pad to maintain body temperature. A 3 mm craniotomy was performed over the right motor cortex (-1.2 mm caudal and 0.71 mm lateral from bregma) using a portable dental drill. Bone dust was removed and then the bone flap was carefully removed without damaging the dura. The injury was then generated using a 2 mm stainless steel piston attached to a CCI device (Leica Biosystems, model# 39463920) at 4 m/s velocity, 1.2 mm and 0.9 mm depth, and using an impact duration of 300 ms. After the injury, the skin was sutured using 2-0 coated vicryl sutures (Ethicon, Mokena,

IL, USA). Sham control mice (total $n = 24$) were exposed to a midline skin incision and re-sutured without performing a craniotomy as it is considered a form of mild injury (Cole *et al.*, 2011; Lagraoui *et al.*, 2012).

ADK inhibitor administration

The ADK inhibitor, 5-iodotubericine (5-ITU, Sigma-Aldrich), was administered intraperitoneally at 1.6 mg/kg in 20% DMSO to C57BL/6 mice (total $n = 12$, six/group) after exposure to moderate TBI. Each animal received five 5-ITU injections, twice daily (at Days 1 and 2 after TBI) and once on Day 3 after TBI (2 h before perfusion). Control mice received intraperitoneal injections of 20% DMSO at the same time points.

Western blots

Gestational tissues were collected at different developmental stages (E5, E10, E15, E20) from pregnant C57BL/6J mice (total $n = 16$). Pregnant mice were rapidly sacrificed by cervical dislocation, followed by dissecting out individual foetuses from both uteri. Foetal brain was immediately extracted, frozen in liquid nitrogen vapour and stored at $-80°C$. The age of gestational tissues was assessed as previously described (Bolon , 2015). For postnatal (P4, P8) and adult tissues (total $n = 22$), brains were extracted after rapid cervical dislocation of the mice. The total cerebrum was immediately dissected and frozen in liquid nitrogen vapour, then stored at $-80°C$. Brain samples were homogenized in radioimmunoprecepitation assay buffer (RIPA) containing protease inhibitors (Sigma-Aldrich, St. Louis, MO, USA). Protein content was assessed using a Thermo Fisher BCA Protein assay kit. For electrophoresis, 20 μg of aqueous protein extracts were loaded and separated on 10% sodium dodecyl sulfate polyacrylamide gel electrophoresis (SDS-PAGE) gels and transferred to polyvinylidene fluoride (PVDF) membranes (Bio-Rad). The blots were probed overnight at $4°C$ in Tris buffered saline (TBS) (20 mM Tris, 150 mM NaCl, 0.1% Tween, pH 7.5) containing 3% non-fat dry milk, and polyclonal rabbit anti-ADK (Bethyl Labs, A304-280A, 1:4500). The membranes were washed in TBS, and then incubated in TBS containing 5% non-fat dry milk, 1% BSA and goat anti-rabbit secondary antibody (Thermo Fisher Scientific, G-21234, 1:10 000). Immunoreactivity was scanned using a Bio-Rad Touch imager and digitized using Bio-Rad Image Lab software. The ratio of ADK-L over ADK-S expression was determined by quantitative analysis of the western blot bands using Image J V. 1.52 software and expressed as the ratio of optical densities of ADK-L/ADK-S bands. All values are presented as mean ± SEM ($n = 4–8$ mice per age group). One-way ANOVA with Tukey's Multiple Comparison *post hoc* test ($* = P \leq 0.05, ** = P \leq 0.01, *** = P \leq 0.001, **** = P \leq 0.0001$ for significance).

Immunohistochemistry of mouse brain

Animals were anaesthetized and transcardially perfused with 30 ml 1× cold phosphate buffered saline (pH 7.4), followed by 30 ml ice-cold 4% paraformaldehyde (PFA). Brains were post-fixed for 24 h in 4% PFA. Following post-fixation, brains were transferred to 30% sucrose with 0.1% sodium azide in 1× PBS for 2 days at $4°C$ and stored at $-80°C$. Brains were then cut coronally or sagittally into 30 μm sections on a freezing, sliding stage cryostat (Leica CM3050S). Until further processing, all sections were stored in cryoprotectant. Immunohistochemistry of mouse brain was performed on free-floating sections. For immunofluorescence, sections were washed in 1× TBS (Tris-Buffered Saline) and 0.05% Triton X-100 (TBS-T) three to four times. Sections were then incubated at $4°C$ overnight in Donkey blocking buffer containing corresponding primary antibodies. The primary antibodies used were monoclonal mouse anti- Glial fibrillary acidic protein (GFAP) (Millipore, MAB360, 1:1000), polyclonal goat anti-doublecortin (DCX) (santa Sruze Biotech, SC8066, 1:1000), polyclonal rabbit anti-ADK (Bethyl Labs, A304-280A , 1:1000) and monoclonal rat FITC conjugated anti-Ki67 (Thermo Fisher, 11-5698-82,1:200). Sections were washed in 1× TBS-T, incubated for 1 h at room temperature in a solution containing the corresponding secondary antibodies. Secondary antibodies included Donkey Alexa Fluor 488 (Thermo Fisher, A-21202, 1:1000), Donkey Alexa 555 (Thermo Fisher, A-21432, 1:1000) and Donkey Alexa Fluor 647 (Abcam, ab150075). Sections were then washed three times for 5 min in 1× TBS then mounted on slides and allowed to dry in the dark. Once dried, sections were cover-slipped with DAPI mounting medium and stored in the dark at $4°C$.

For the 3,3′-diaminobenzidine (DAB) staining, frozen sections were washed five times for 5 min in PBS-T then quenched in 0.3% H_2O_2 for 30 min. Sections were then washed three times in PBS-T at room temperature then blocked for one hour in goat blocking buffer (GBB). Sections were then incubated overnight at $4°C$ in GBB containing the primary antibody, polyclonal rabbit anti-ADK (Bethyl Labs, A304-280A , 1:1000). Sections were washed three times with TBS and then incubated in GBB containing biotinylated goat anti-rabbit IgG (1:5000) secondary antibody. After three washes in PBS-T, sections were incubated in avidin–biotin horseradish peroxidase complex solution, then in DAB substrate solution (Vector Laboratories, SK-4105) for up to 10 min until the reaction product visualized. Sections were washed three times for 5 min in PBS-T then mounted on slides and allowed to dry. Sections were dehydrated in alcohol, cleared in xylene and mounted with mounting medium (Fisher Scientific, SP15-100 UN1294).

Image acquisition and cell counting

The 3,3′-diaminobenzidine images in Figs 1 and 2 were acquired on a Lica light micropscope (Leica DM 4B).
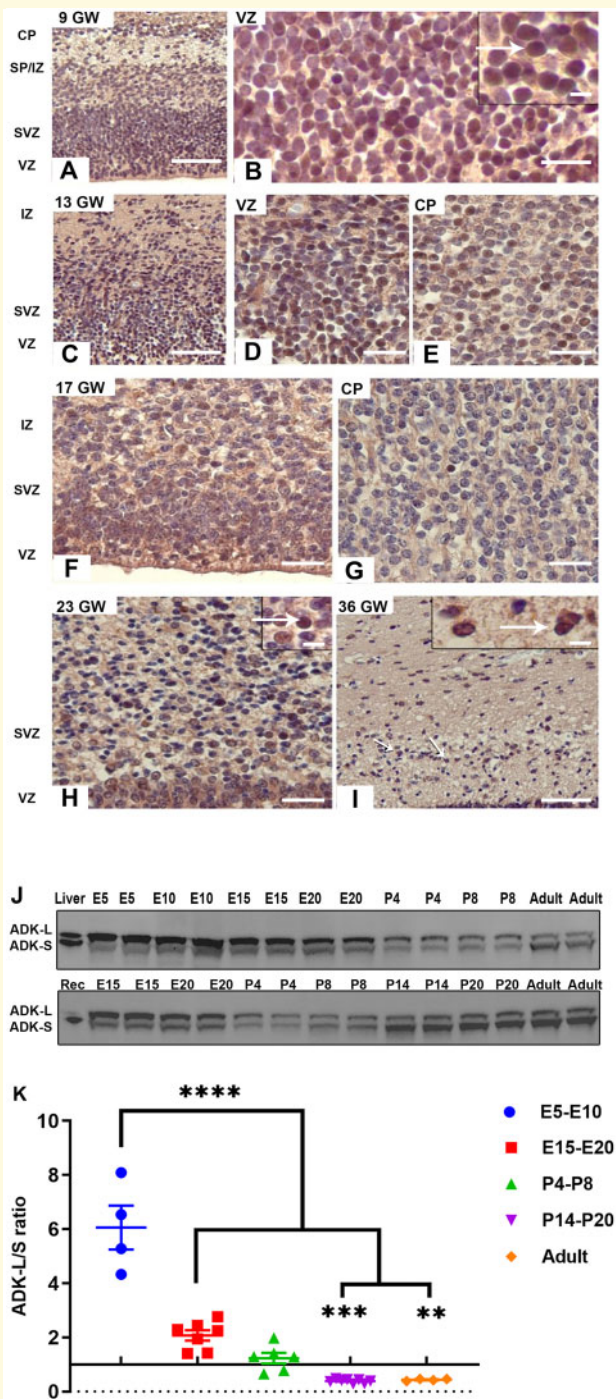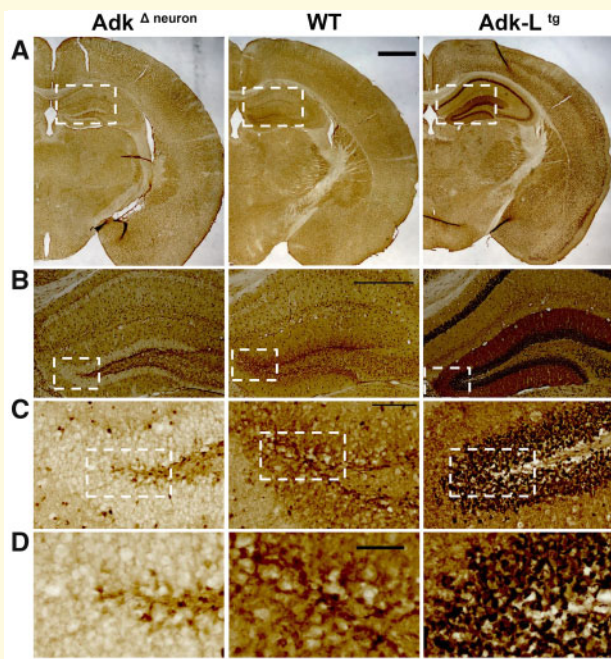
Figure 1 ADK immunoreactivity in developing human and mouse brains. (A–I) ADK immunoreactivity (IR) in human specimens at different ages (9, 13, 17, 25 and 36 GWs). **(A–B)** 9 GW. **(A)** ADK IR is observed in the VZ, SVZ and the CP. High magnification photographs show ADK-positive cells in the VZ (**B** and insert in **B**). **(C–E)** 13 GW, showing ADK nuclear expression in SVZ/VZ and CP. **(D)**: high magnification photograph of VZ; €: high magnification photograph of CP. **(F–G)** 17 GW with ADK IR in the SVZ/VZ (**F**), but decreased expression in the CP (**G**). **(H)** 25 GW with still detectable ADK expression in the SVZ/VZ; insert in **H** shows high magnification of positive cells within the SVZ. **(I)** 36 GW: the SVZ contains ADK-positive cells (high magnification in insert). VZ: ventricular zone; SVZ: subventricular zone; SP/IZ: subplate/intermediate zone; CP: cortical plate. Scale bars are 100 μm in **A, C and I**; 25 μm in **B**; 40 μm in **D–H** and 7.5 μm in inserts in **B, H and I**. **(J)** Expression profile of ADK-L and ADK-S proteins in developing mouse brain. Western Blot analysis of ADK expression changes during pre- and postnatal brain development in the mouse. Representative blots show ADK (L and S) isoform expression at different embryonic (E) and postnatal (P) stages with ADK-L appearing as the upper band and ADK-S as the lower band. Protein extracts were prepared from total cerebrum at all ages. The long nuclear form of ADK-L dominates during embryonic brain development and shifts towards an ADK-S dominance in the adult brain during postnatal brain development. Controls include liver (organ with the highest concentration of ADK) and recombinant ADK-S (Rec). The original full-sized uncropped blots are shown in Supplementary Figures 1 and 2. **(K)** Quantitative analysis of the Western blot bands using Image J V. 1.52 software and expressed as the ratio of optical densities of ADK-L/ADK-S bands. All values are presented as mean ± SEM ($n = 4$–8). One-way ANOVA with Tukey's multiple comparison *post hoc* test (** $= P < 0.01$, *** $= P < 0.001$, **** $= P < 0.0001$ for significance).

Fluorescence images were acquired on a Leica TCS SPE confocal laser scanning microscope (LAS X 3.1.2.16221) using 20× and 63× (for single-cell images) objectives (a 10 μm confocal Z-stack was acquired at 1 μm steps, 600 Hz speed, pinhole 1 AU, gain 599.4, resolution 1024× 1024). Fluorescence images in Figs 3, 4, 5, 6 and 7 are presenting single channel as well as composites (4th lane in Figs 3A and 6A and in Fig. 4D). For image analysis we selected four 30 μm sections from each stain from each mouse, spaced every 90 μm and spanning an identical caudo-rostral location (spanning from 1.31 mm to 2.27 mm posterior to bregma) between animals ($n = 4$–7 animals per genotype). Different stains (e.g. DCX/GFAP and DCX/Ki67) were always done on adjacent brain sections. Total DCX cell counts were added from respective double immunofluorescence stainings. An unbiased exclusion of images of poor quality was made prior to the analysis by a person who was blinded to the animal groups. Automated cell counting was performed by an individual blinded to the genotypes and phenotypes. The borders of the deep internal layer (subgranular layer) of the DG and hilus were highlighted as region of interest (ROI). For DCX counting, cells in subgranular and granular interface were defined as previously published (Hattiangady *et al.*, 2008; Long *et al.*, 2017)

Binarization of DCX-, Ki67-, ADK-, and GFAP-stained images was performed using the ImageJ software Auto Threshold command (ImageJ, US National Institutes of Health, Bethesda, MD, USA; http://imagej.nih.gov/ij/). For each stain, the optimal threshold values were achieved by manually adjusting the range of pixel intensity on an initial set of images (Crews *et al.*, 2006). The determined range of pixel intensities was then applied for the rest of the set of images, remaining consistent throughout all sections. The ImageJ watershed algorithm was applied to DCX-, ADK-, and GFAP-stained images to cut between adjacent cells. Using the 'particle analysis' command, the total number of

Figure 2 Characterization of ADK expression profile in brains of naïve Adk-L[tg], Adk[Δneuron], and control animals.
(**A**) ADK immunoreactivity (IR) as shown by peroxidase-DAB immunohistochemistry in coronal sections of adult male Adk-L[tg] and Adk[Δneuron] mice is compared with WT-littermate controls from Adk[Δneuron] × *Adk*-flox matings. According to prior studies WT animals show typical widespread ADK IR throughout the entire brain. Note prominent ADK-IR in the dentate granular cell layer. Adk[Δneuron] mice look almost identical compared to WT, however with a distinct lack of ADK-IR in the dentate granular layer, which appears as white blades. In contrast, Adk-L[tg] mice show prominent expression of ADK-L in cortical neurons, including neurons of the dentate gyrus as well as the pyramidal cell layer, which normally does not express ADK. (**B–D**) Higher magnifications reveal a typical pattern of ADK expression with widespread astrocytic ADK-S in the cytoplasm appearing as brown background and ADK-L appearing as black punctate demarcating nuclei of astrocytes and neurons from the dentate granular layer. Sections from Adk[Δneuron] mice look almost identical, however with a distinct lack of ADK-IR in dentate granular neurons. Sections from Adk-L[tg] mice show strong ectopic immunoreactivity of ADK-L in neurons of the dentate granular zone and the pyramidal cell layer, Scale bar is 1 mm in **A**, 500 μm in **B**, 100 μm in **C** and 50 μm in **D**.

cells in the ROI was automatically quantified. In the interest of avoiding unwanted noise and/or background pixels, a range of particle characteristics for automatic quantification was determined from binary image data for each stain. Cell counts were quantified as cell number per mm² and normalized to that of the corresponding WT control.

Statistical analyses

Statistical analyses were performed using GraphPad Prism7.04. Data are expressed as mean ± SEM. Statistical significance was set as $P < 0.05$. Two-tailed unpaired Student *t*-tests were used for experiments with two groups and one variable. One-way ANOVA with Tukey's *post hoc* test was used for experiments with three groups and one variable.

Data availability

All data and resources will be made available upon request.

Results

## ADK expression during foetal human brain development

Because ADK expression in the adult brain is limited to cell types, which maintain plasticity and proliferative capacity, such as astrocytes and a limited number of neurons in neurogenic zones (Studer *et al.*, 2006; Boison, 2013; Kiese *et al.*, 2016), we hypothesized that ADK expression is more widespread during gestational brain development. We therefore studied ADK expression in a set of foetal brain specimens obtained from spontaneous or medically induced abortions (Fig. 1A–I). During GW9, we found widespread ADK immunoreactivity in the ventricular zone, subventricular zone and cortical plate. At GW13, we found strong expression of ADK maintained in cell nuclei of those brain regions. At GW17, ADK immunoreactivity was maintained in the ventricular and subventricular zone; however, we found decreased expression in the cortical plate. At GW25, ADK expression was reduced, but still detectable in the ventricular and subventricular zone. At GW36, ADK-positive cells were limited to the subventricular zone. This developmental profile shows a gradual decline in neuronal ADK expression during the progression of foetal brain development, while the expression of ADK was maintained longest in nuclei of cells from the subventricular zone, suggesting an association of ADK-L with neurogenic zones in the developing human brain.

ADK expression during foetal and postnatal mouse brain development

To determine whether developmental changes of ADK expression during human brain development are replicated during the development of the mouse, we performed a Western blot analysis (Fig. 1J) to distinguish the two isoforms of ADK by size in the brain of mouse at different developmental stages. During embryonic mouse brain development, we found a dominance of ADK-L over ADK-S expression with the ADK-L/ADK-S ratio gradually declining over time. Postnatally, we found a shift in the expression ratio to transition into the adult expression pattern of ADK-S dominance over ADK-L (Fig. 1K). We conclude that ADK-L expression is associated with brain growth and development.
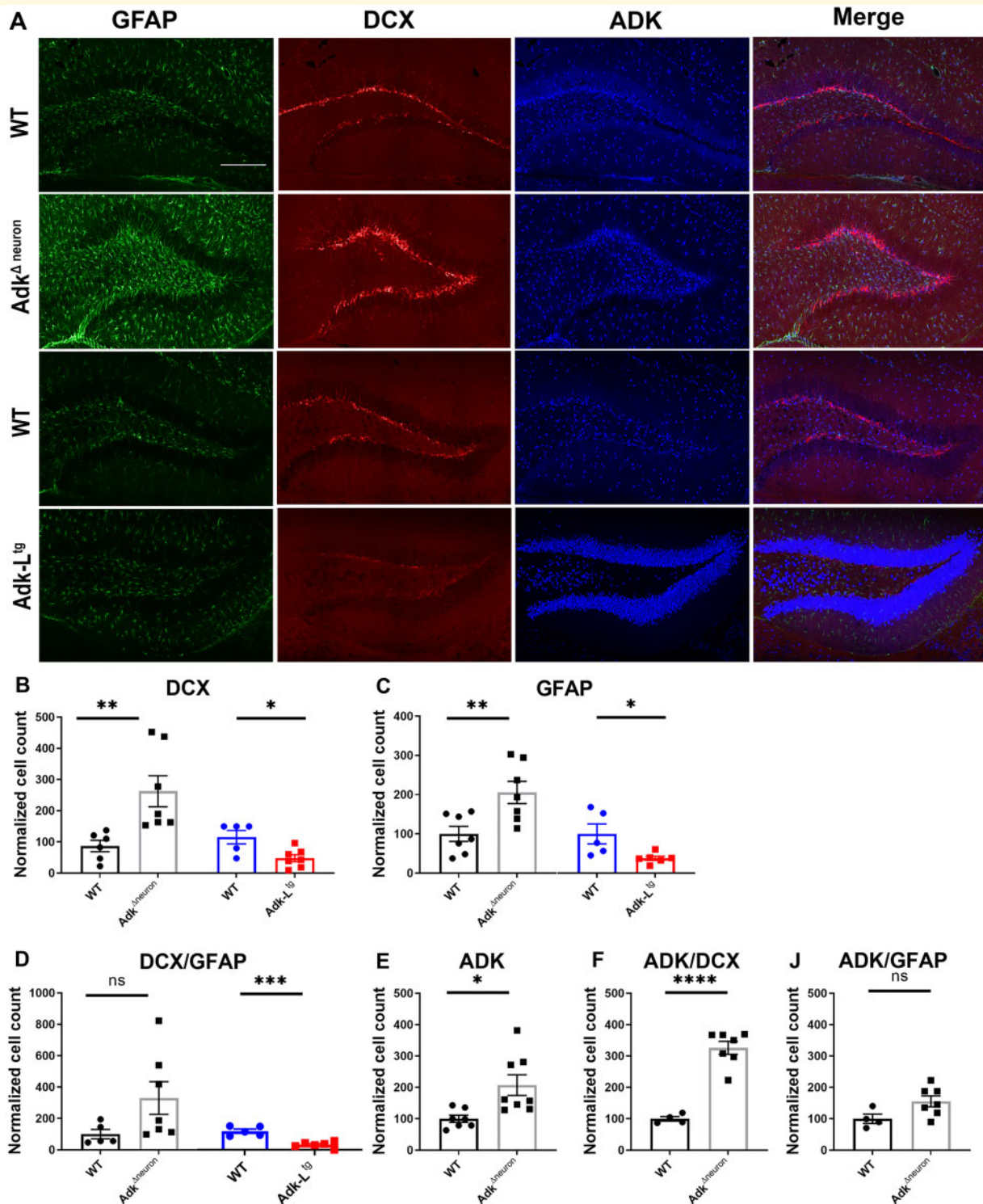
Figure 3 ADK-L modulates TBI-induced expression of neurogenic markers. (A) Immunofluorescence of DCX, GFAP, and ADK in the DG ipsilateral to the injury of Adk$^{\Delta neuron}$ and Adk-L^{tg} mice compared to their respective littermate WT controls at 3 days post injury. **(B–J)** Quantitative analysis of neurogenic and ADK-positive cell populations in the DG and hilus (ipsilateral to the CCI) of both transgenic lines (Adk-L^{tg}, Adk$^{\Delta neuron}$) per mm^2 normalized to their respective littermate WT control and presented as percentage of fold change. **(B)** Relative number of DCX-positive cells normalized to WT. **(C)** Relative number of GFAP-positive cells normalized to WT. **(D)** Relative number of cells double-labelled for DCX and GFAP normalized to WT. € Relative number of ADK-positive cells in Adk$^{\Delta neuron}$ mice normalized to WT. **(F)** Relative number of cells double-labelled for ADK and DCX in Adk$^{\Delta neuron}$ mice normalized to WT. **(J)** Relative number of cells double-labelled with ADK and GFAP in Adk$^{\Delta neuron}$ mice normalized to WT. Scale bar is 200 μm in **A.** All values are presented as mean ± SEM ($n = 5$–9 mice per genotype). Two-tailed unpaired Student t-tests were used in **B-J**. *$P \leq 0.05$, **$P \leq 0.01$, ***$= P \leq 0.001$, NS = no significance.
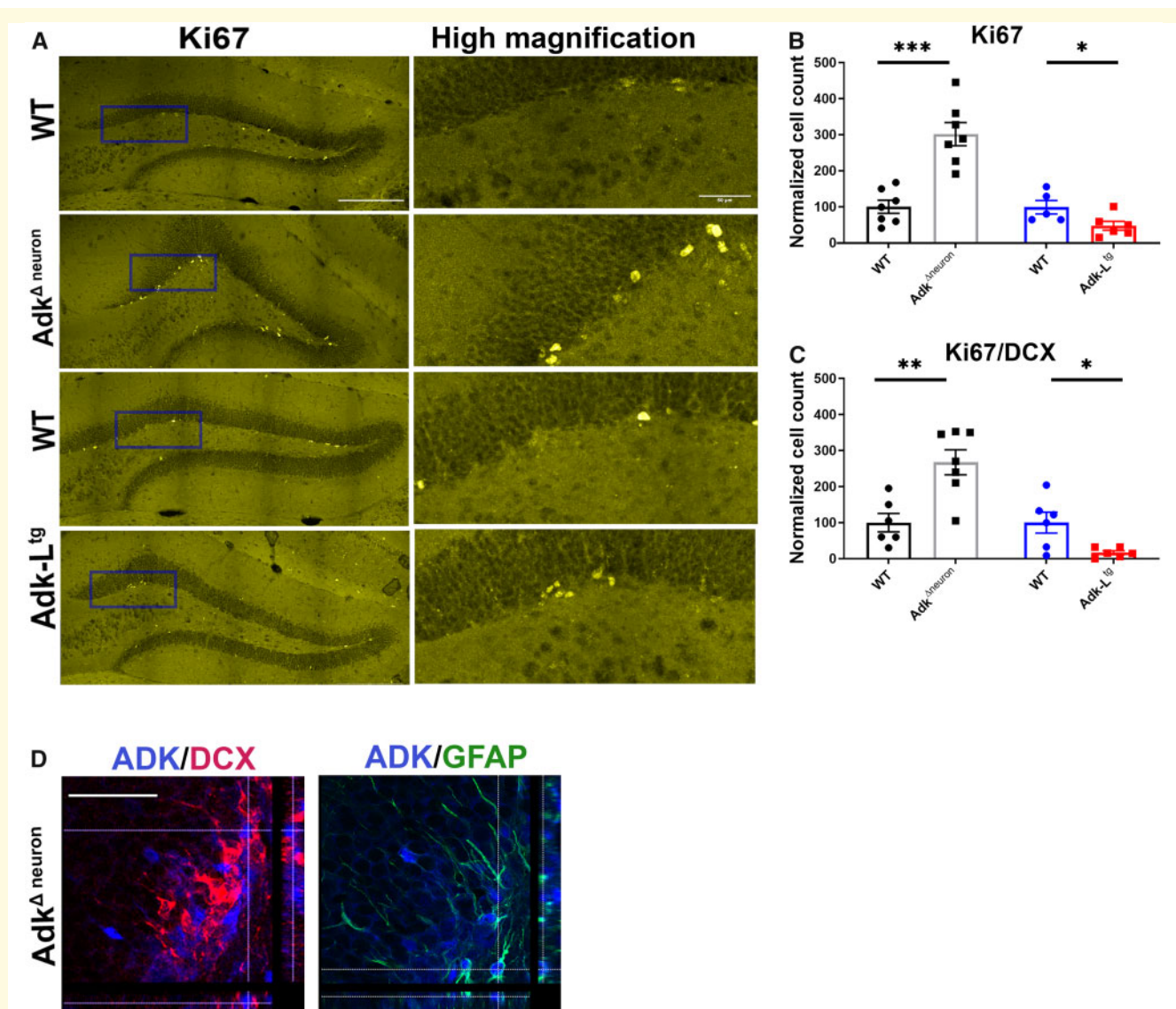
Figure 4 ADK-L modulates TBI-induced cell proliferation. (A) Immunofluorescence of the cell proliferation marker Ki67 in Adk-L[tg] and Adk[Δneuron] mice compared with respective WT littermate controls at 3 days post injury; a magnified image of proliferative cells is shown in the close-ups. **(B)** Relative number of Ki67-positive cells normalized to WT. **(C)** Relative number of cells double labelled for Ki67 and DCX normalized to WT. **(D)** Confocal images with orthogonal projections illustrating the identity of ADK-positive cells in Adk[Δneuron] mice (DCX-positive cells co-express ADK (top) and GFAP-positive cells co-express ADK (bottom)). Scale bar is 200 μm in **A** and 50 μm in **D**. All values are presented as mean ± SEM ($n = 5$–9 mice per genotype). Two-tailed unpaired Student *t*-tests were used in **B and C**. *$P \leq 0.05$, **$P \leq 0.01$, ***= $P \leq 0.001$, NS = no significance.

Transgenic manipulation of ADK-L

To investigate the functional implications of ADK-L expression for brain development and plasticity, we engineered a set of transgenic mice that either lack or overexpress ADK-L in neurons of the forebrain. To accomplish this, we used an identical CamKIIα-promoter to drive the expression of Cre-recombinase in conditional Adk-flox mice or to ectopically overexpress ADK-L in adult neurons of the forebrain resulting in ADK[Δneuron] and ADK-L[tg] mice, respectively. Engineered changes of ADK expression in the forebrain were qualitatively evaluated through analysis of ADK immunoreactivity on brain sections (Fig. 2). According to our prior work (Gouder *et al.*, 2004; Studer *et al.*, 2006), WT mice (Fig. 2, centre) showed global astrocytic ADK-S expression, which appears as diffuse staining throughout the entire brain, with ADK-L appearing as dark punctate staining in nuclei. We found moderate

expression levels of ADK-L in nuclei of DG neurons. Because DG neurons are the only neurons that express ADK in the adult cortex and hippocampus, the CamKIIα-Cre-driven deletion of the *Adk*-gene in ADK$^{\Delta neuron}$ mice resulted in an almost identical staining pattern (astrocytic ADK expression was not affected) except the lack of ADK-L in DG neurons (Fig. 2, left). In contrast, ADK-L^{tg} mice showed robust ectopic expression of ADK-L in nuclei of neurons throughout the forebrain (Fig. 2, right).

Genetic disruption of ADK-L enhances TBI-induced neural stem cell proliferation

TBI is an important trigger of endogenous neural stem cell proliferation in the hippocampus (Dong *et al.*, 2015; Bang *et al.*, 2016; Neuberger *et al.*, 2017). Because ADK-L expression is associated with plastic and proliferative areas of the brain, we assessed whether ADK-L plays a role in the regulation of post-injury neural stem cell proliferation. Animals of all genotypes were subjected to moderate-to-severe TBI using a CCI (total $n = 28$). Because CCI-induced neural stem cell proliferation peaks at 3 days after injury (Dash *et al.*, 2001), we evaluated TBI-induced endogenous neural stem cell proliferation in DG by quantifying the expression of doublecortin (DCX), glial fibrillary acidic protein (GFAP) and Ki67 at this time point by immunohistochemistry and cell counting (Figs. 3A and 4A). We quantified DCX, GFAP and Ki67-positive cells in the neurogenic area of the DG in adult naïve ADK$^{\Delta neuron}$ positive for DCX ($P < 0.01$) (Fig. 3B), GFAP ($P < 0.009$) (Fig. 3C), and Ki67 ($P < 0.0001$) (Fig. 4B). Because neurogenesis in the adult hippocampus occurs in the subgranular zone, we specifically quantified ADK-L expressing cells in this area of the DG (Fig. 3E–J). Of note, the genetic manipulation under the control of CamKIIα-promoter induces the ADK-L gene disruption only in adult neurons and is not expected to affect the genetic profile of neural stem cells in the SGZ. As expected, ADK$^{\Delta neuron}$ mice lacked ADK expression in DG neurons; however, the number of ADK-L-positive cells in the adjacent SGZ was increased compared to WT ($n = 6$–9; $P < 0.012$). Importantly, in ADK$^{\Delta neuron}$ mice the expression of ADK-L in the subgranular zone was co-localized with DCX (Fig. 4F). The number of cells double-labelled with ADK and DCX was increased more than 3-fold ($P < 0.0001$) compared to WT ($n = 4$–7). We further validated these findings by assessing TBI-induced neural stem cell proliferation in transgenic animals overexpressing ADK-L in dorsal forebrain neurons (ADK-L^{tg}). As expected, ADK-L^{tg} mice ($n = 6$–7) showed an opposite phenotype with slight decreases in the expression of DCX ($P = 0.013$) (Fig. 3B), Ki67 ($P = 0.04$) (Fig. 4B) and GFAP ($P = 0.02$) (Fig. 3C). Together, these results suggest a role of ADK-L in the modulation of endogenous neural

stem cell proliferation after TBI and provide a rationale for the therapeutic use of ADK inhibitors to boost endogenous neural stem cell proliferation after a TBI.

Pharmacological blockade of ADK enhances neural stem cell proliferation after TBI

To further validate ADK-L effects on TBI-induced neural stem cell proliferation and to confirm our results from the ADK$^{\Delta neuron}$ mice, a total of five injections of the potent ADK inhibitor 5-ITU (1.6 mg/kg i.p.), or vehicle, were administered every 12 h following a TBI in adult male WT C57BL/6 mice ($n = 4$–6/group) (Fig. 5A). This dose has previously been shown to induce potent disease-modifying effects in an epilepsy model in mice (Sandau *et al.*, 2019). Three days after the TBI, we quantified DCX- and Ki67-positive cells in 5-ITU injected animals and compared them with vehicle-treated animals (Fig. 5B). In line with our findings from the ADK$^{\Delta neuron}$ mice, we found significant increases in DCX- and Ki67-positive cells ($P = 0.002$ and $P = 0.03$, respectively) in the 5-ITU treated group compared to control (Fig. 5C and D). These results validate our experiments from the transgenic animals and demonstrate that the pharmacological inhibition of ADK is an approach to enhance neural stem cell proliferation and cell proliferation after TBI.

ADK-L disruption affects baseline neural stem cell proliferation

To rule out possible adverse effects of ADK-L blockade in non-injured animals, we next assessed the effects of ADK-L blockade on endogenous baseline neural stem cell proliferation under physiological condition in non-injured transgenic animals. We quantified DCX, GFAP and Ki67-positive cells in the neurogenic area of the DG in adult naïve ADK$^{\Delta neuron}$ and ADK-L^{tg} mice in comparison to WT controls ($n = 4$–6/each line) (Figs 6 and 7). Compared to WT we found no significant impact on the number of DCX-positive cells ($P = 0.08$) in the ADK$^{\Delta neuron}$ mice whereas both DCX (Fig. 6B) and Ki67- (Fig. 7B) positive cells were increased 2-fold in the DG of ADK-L^{tg} mice ($P < 0.0001$ and $P < 0.04$, respectively) (Fig. 7B). Those results demonstrate that ADK-L disruption has selective effects on neural stem cell proliferation in the injured and non-injured brain.

Traumatic brain injury impacts ADK effect on adult neural stem cell proliferation

To investigate the effect of TBI, we compared cell counts of DCX, ADK, GFAP and Ki67 cell populations in both transgenic lines and each was normalized to its corresponding WT (Fig. 7D–J). Interestingly, as compared to
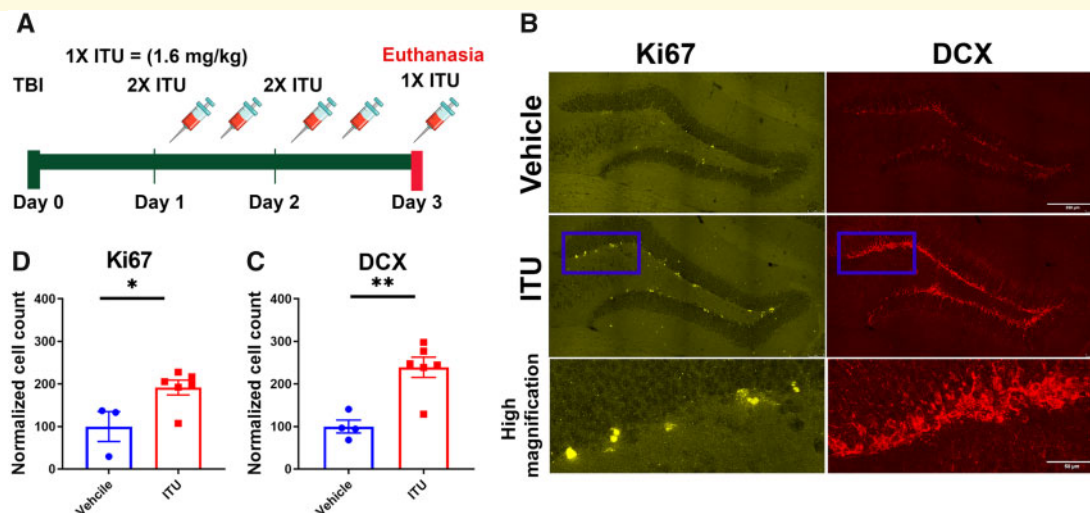
Figure 5 Pharmacological inhibition of ADK-L enhances TBI-induced neural stem cell proliferation. (A) WT C57BL/6 mice were treated with five intraperitoneal injections of either 5-iodotubercidin (5-ITU) or vehicle (20% DMSO) 24 h after the TBI. **(B)** Immunofluorescence of DCX and Ki67 in the DG ipsilateral to the injury of 5-ITU- and vehicle-treated control mice. A magnified field of proliferative and neurogenic areas of ITU-treated mice is presented in the third row. **(C)** Relative number of DCX-positive cells normalized to control. **(D)** Relative number of Ki67-positive cells normalized to control. Scale bar is 250 μm in first and second rows, 50 μm in the third row. All values are presented as mean ± SEM ($n = 3–6$ mice per genotype). Two-tailed unpaired Student t-tests were used in **C** and **D**. $*P \leq 0.05$, $**P \leq 0.01$.

naïve group, there is significant increase in DCX ($P = 0.003$), ADK ($P = 0.02$), GFAP ($P = 0.005$) and Ki67 ($P < 0.0001$) in injured ADK$^{\Delta neuron}$ mice (Fig. 7D–G). In line with these findings, we found significant reduction in DCX ($P < 0.0001$), GFAP ($P = 0.0009$) and Ki67 ($P < 0.0014$) in injured ADK-L^{tg} mice (Fig. 7H–J). These results confirm an association of TBI with ADK effect on the activity of DG cells population.

Discussion

Here we identified a novel role of ADK in the regulation of neural stem cell proliferation and cellular plasticity, which is of relevance for brain development and responses to injury. First, using human and murine foetal and postnatal brain, we show an association of the nuclear expression of ADK in neurons with neurogenic brain areas and developmental stages characterized by cell proliferation. Secondly, using genetic manipulation of ADK-L in the nuclei of neurons we show that ADK-L modulates neural stem cell proliferation after TBI. Thirdly, we demonstrated that the pharmacological inhibition of ADK enhanced neural stem cell proliferation in the injured brain.

Role of ADK in brain development

In line with previous findings suggesting a dual functionality of ADK (Studer et al., 2006), we find matching and coordinated changes in the ADK expression profile during both human and murine brain development. Our data are in line with gene expression profile changes in the mouse showing a rapid drop in neuronal ADK-L transcripts and a rise in astroglial ADK-S transcripts during the first 2 weeks of postnatal brain development (Kiese et al., 2016). Those findings and our current data (Fig. 1) support the view that ADK-L, expressed in the nuclei of neurons and immature precursor cells plays a critical role in embryonic and early postnatal brain development. A developmental role for ADK is supported by human mutations in the Adk gene (Bjursell et al., 2011; Staufner et al., 2016). Affected individuals present with global developmental delay, cognitive impairment and seizures commencing between the first and third year of life (Bjursell et al., 2011; Staufner et al., 2016). In line with the human subjects, Nestin-Cre: Adk-flox mice show a brain-wide deletion of Adk beginning around embryonic Day 11 (Sandau et al., 2016), show neuronal plasticity changes resulting in stress-induced epileptic seizures, and deficits in social memory and contextual learning, whereas the postnatal disruption of ADK expression in most areas of the brain did not result in those behavioral deficits and seizures (Osborne et al., 2018). Those findings suggest that developmental ADK-L expression changes described here might play a critical role in brain development. Of note, neuropsychiatric conditions, such as autism and schizophrenia, with a developmental aetiology might result from an imbalance in adenosine homeostasis (Boison et al., 2012; Shen et al., 2012; Masino et al., 2013; Chen et al., 2014).
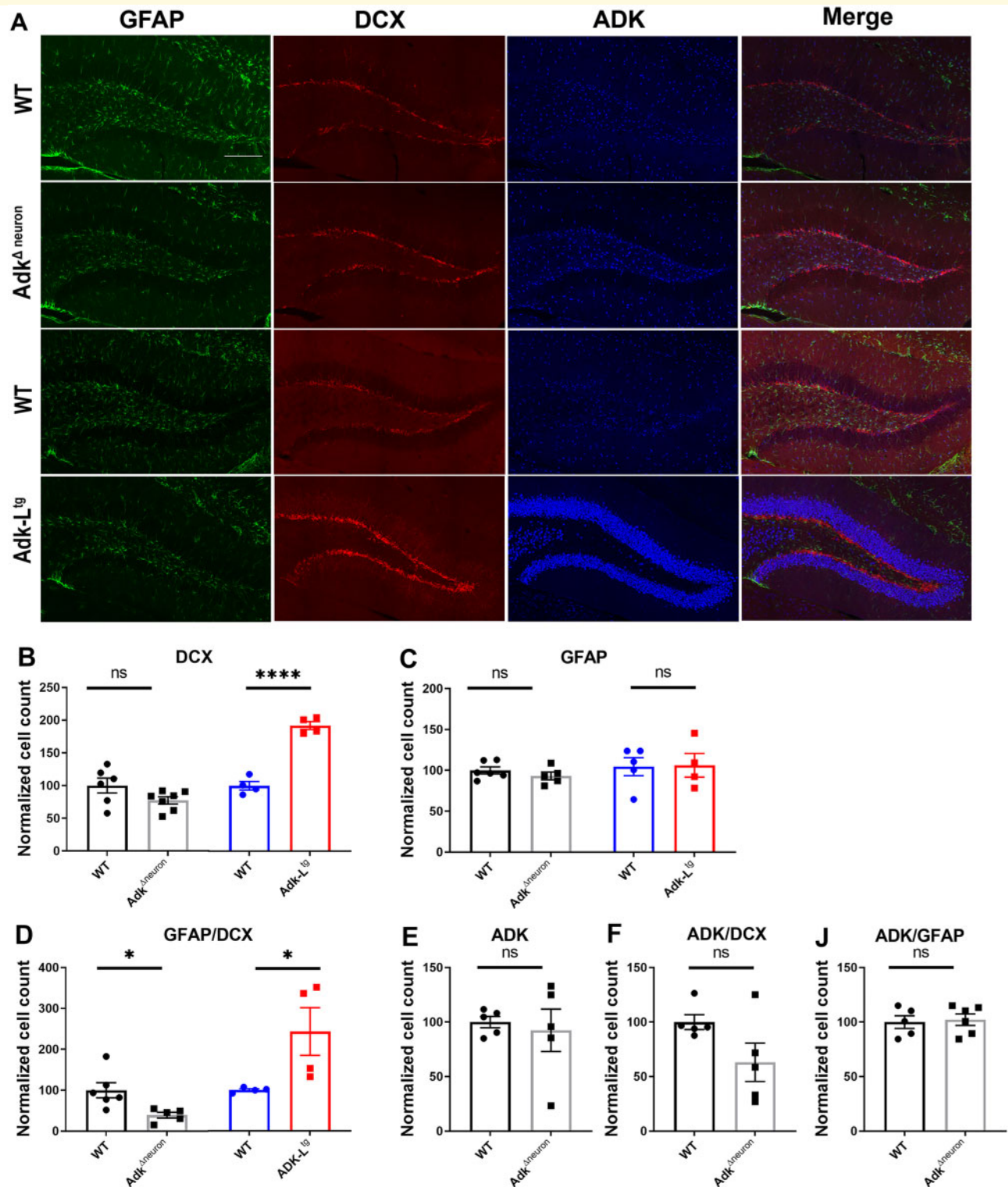
Figure 6 Baseline neurogenic cell population in naïve Adk$^{\Delta neuron}$, Adk-L^{tg} and WT animals. (A) Immunofluorescence of GFAP, DCX, and ADK in the DG of Adk-L^{tg}, Adk$^{\Delta neuron}$ and littermate WT controls for each of the transgenic lines. Scale bar is 200 μm. (B–J) Quantitative analysis of neurogenic and ADK-positive cell populations in DG and hilus of both transgenic lines (Adk-L^{tg}, Adk$^{\Delta neuron}$) and Adk$^{\Delta neuron}$ mice, respectively. Cell counts per mm^2 in the transgenic animals were normalized to their respective littermate WT control and presented as percentage of fold change. (B) Relative number of DCX-positive cells normalized to WT. (C) Relative number of GFAP-positive cells normalized to WT. (D) Relative number of cells double-labelled with DCX and GFAP normalized to WT. (E). Relative number of ADK-positive cells in Adk$^{\Delta neuron}$ mice normalized to WT. (F) Relative number of cells double-labelled with ADK and DCX in Adk$^{\Delta neuron}$ mice normalized to WT. (J) Relative number of cells double-labelled with ADK and GFAP in Adk$^{\Delta neuron}$ mice normalized to WT. Scale bar is 200 μm. All values are presented as mean ± SEM ($n = 4$–6 mice per genotype). Two-tailed unpaired Student t-tests were used in **B-J**. *$P \leq 0.05$, ***$= P \leq 0.001$, ns = no significance.
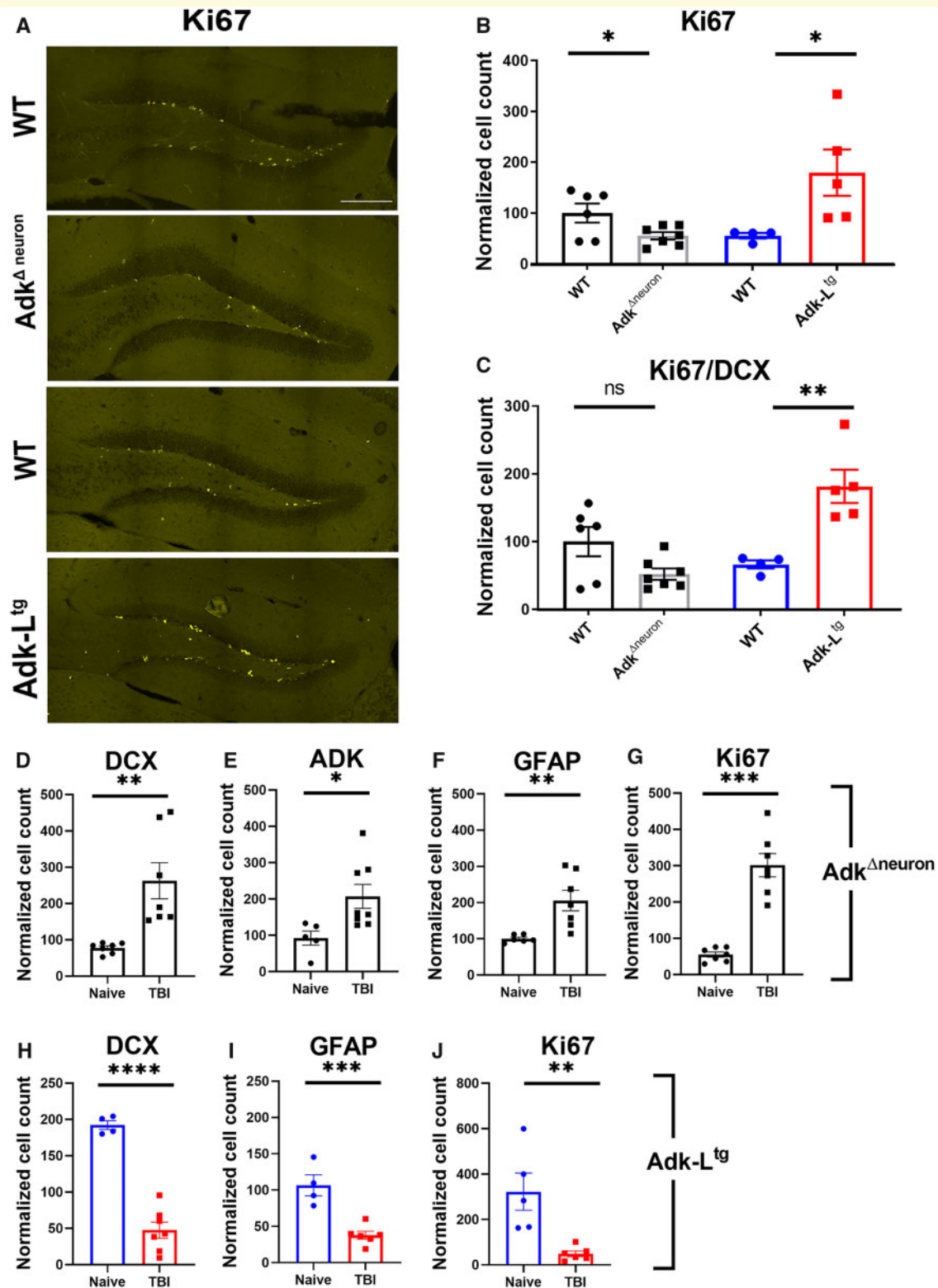
Figure 7 Baseline cell proliferation in naïve Adk$^{\Delta neuron}$, Adk-L^{tg} and WT animals. (A) Immunoreactivity of the cell proliferation marker Ki67 in naïve Adk-L^{tg}, Adk$^{\Delta neuron}$, and littermate WT controls. Scale bar is 200 μm. (B–C) Quantitative analysis of all proliferative and DCX-positive proliferative cell populations in DG and hilus of both transgenic lines (Adk-L^{tg}, Adk$^{\Delta neuron}$). (B) Relative number of Ki67-positive cells normalized to WT. (C) Relative number of Ki67- and DCX-positive cells normalized to WT. (D–J) Quantitative analysis of DG cell populations in injured versus uninjured transgenic mice lines. (D, E, F and G) Relative number of DCX, ADK, GFAP and Ki67-positive cells, respectively, in Adk$^{\Delta neuron}$ mice normalized to WT. (H, I and J) Relative number of DCX, GFAP and Ki67-positive cells, respectively, in Adk^{tg} mice normalized to WT. Scale bar is 200 μm. All values are presented as mean ± SEM ($n = 4$–6 mice per genotype). Two-tailed unpaired Student *t*-tests were used in **B & C**. *$P \leq 0.05$, **$P \leq 0.01$, ***$= P \leq 0.001$, ****$= P < 0.001$, ns = no significance.

Role of ADK in adult neural stem cell proliferation

In adulthood, neural stem cell proliferation is maintained only in a few areas of the brain including the subgranular zone of the DG (Parent, 2007; Toda *et al.*, 2019). Interestingly, and in contrast to mature neurons throughout the rest of the brain, ADK-L expression is maintained in DG neurons (Fig. 2). Injuries to the brain, in particular prolonged epileptic seizures, stroke, or TBI, are potent triggers of adult neural stem cell proliferation in the DG (McGeer *et al.*, 2003; Dudek and Sutula, 2007; Kernie and Parent, 2010; Burda *et al.*, 2016). To assess a functional role of ADK-L for injury-induced neural stem cell proliferation, we used a set of transgenic mice with reciprocal changes in hippocampal ADK-L expression: ADK-L^{tg} mice with ectopic expression of ADK-L in adult neurons of the forebrain, including a marked overexpression of ADK-L in DG neurons; and ADK$^{\Delta neuron}$ mice, with a deletion of ADK-L in DG neurons (and lack of ADK-L in all other forebrain neurons). Here we show that the genetic modulation of ADK-L expression has a robust effect on TBI-induced neural stem cell proliferation. In contrast to our findings on baseline neural stem cell proliferation in non-injured animals (Fig. 6), we found that 3 days after TBI, neural stem cell proliferation in the DG was robustly stimulated in ADK$^{\Delta neuron}$ mice. Importantly, neural stem cell proliferations and cell proliferation in ADK$^{\Delta neuron}$ mice was associated with increased expression of ADK-L in the subgranular zone and hilus (Figs 3 and 4D). Most of the ADK-positive cells were also GFAP-positive and the rest were DCX-positive cells (Fig. 3D). We propose that the lack of ADK-L in DG neurons might lead to compensatory increases in ADK-L expression in neurogenic zones, implicating a direct role of ADK-L for neural stem cell proliferation.

Under physiological conditions, we found an association of ADK-L expression with the proliferative status of neurogenic cell populations in the DG (Fig. 6). This was shown by the quantitative assessment of Ki67-positive cells, which revealed more cell proliferation in ADK-L overexpressing transgenic mice, whereas the genetic deletion of ADK-L from DG neurons did significantly impact proliferation. In line with increased baseline neural stem cell proliferation in ADK-L^{tg} mice, we found a significant increase in DCX-positive cells and GFAP/DCX-positive cells. Again, mice with a genetic deletion of ADK-L in the DG showed the opposite effect.

Possible mechanisms

Epigenetic mechanisms, including methylation of DNA in the central nervous system, play a role in activity-induced proliferation of neural precursor cells. In particular, the activity-induced gene *Gadd45b* was shown to play a role in neural stem cell proliferation via determining the methylation status of two seizure-induced genes, *Fgf1* and *Bdnf* (Barreto *et al.*, 2007; Ma *et al.*, 2009). These findings suggest that epigenetic modifications are employed for long-lasting modulation of plasticity after neuronal activity or injury. We recently identified regulation of DNA methylation as a novel function of adenosine (Williams-Karnesky *et al.*, 2013) which provides inhibitory feedback control on the flux of S-adenosylmethionine dependent transmethylation reactions, which include DNA methylation (Boison *et al.*, 2002). In line with this mechanism, we have demonstrated directly that increases in ADK-L expression drive increased DNA methylation (Williams-Karnesky *et al.*, 2013). Because changes in DNA methylation play a role in neural stem cell proliferation, and because the nuclear isoform ADK-L has a specific role to control DNA methylation status, we propose that ADK-L regulates neural stem cell proliferation through an epigenetic mechanism.

Therapeutic perspectives

In line with the genetic deletion of ADK, the pharmacological blockade of ADK resulted in increased neural stem cell proliferation 3 days after TBI (Fig. 5). These findings suggest that pharmacological inhibition of ADK is a viable strategy to modulate neural stem cell proliferation after TBI. One caveat of therapeutic approaches that promote neural stem cell proliferation after brain injuries is the risk for the development of seizures, especially in TBI survivors (Annegers and Coan, 2000). In contrast, the ADK inhibitor 5-ITU has recently been shown to exert antiepileptogenic disease-modifying properties (Sandau *et al.*, 2019), suggesting that 5-ITU is capable of increasing neural stem cell proliferation after a brain injury without the risk of promoting the development of epilepsy.

In summary, the present work describes the discovery of a novel role of ADK-L as regulator of neural stem cell proliferation after injury in the adult brain and provides the rationale for further studies aimed at understanding the underlying epigenetic mechanisms, at assessing potential sex differences and at assessing long-term functional outcomes.

Supplementary material

Supplementary material is available at *Brain Communications* online.

Acknowledgements

Funding

Competing interests

The authors declare that they have no competing interests. D.B. is a co-founder of PrevEp LLC.

References

Aid T, Kazantseva A, Piirsoo M, Palm K, Timmusk T. Mouse and rat BDNF gene structure and expression revisited. J Neurosci Res 2007; 85: 525–35.

Altman J, Das GD. Autoradiographic and histological evidence of postnatal hippocampal neurogenesis in rats. J Comp Neurol 1965; 124: 319–35.

Annegers JF, Coan SP. The risks of epilepsy after traumatic brain injury. Seizure 2000; 9: 453–7.

Bang SA, Song YS, Moon BS, Lee BC, Lee H, Kim J-M. Neuropsychological, metabolic, and GABA A receptor studies in subjects with repetitive traumatic brain injury. J Neurotrauma 2016; 33:

Barreto G, Schäfer A, Marhold J, Stach D, Swaminathan SK, Handa V, et al. Gadd45a promotes epigenetic gene activation by repair-mediated DNA demethylation. Nature 2007; 445: 671–5.

Bjursell MK, Blom HJ, Cayuela JA, Engvall ML, Lesko N, Balasubramaniam S, et al. Adenosine kinase deficiency disrupts the methionine cycle and causes hypermethioninemia, encephalopathy, and abnormal liver function. Am J Hum Genet 2011; 89: 507–15.

Boison D. Adenosine kinase: exploitation for therapeutic gain. Pharmacol Rev 2013; 65: 906–43.

Boison D, Aronica E. Comorbidities in neurology: is adenosine the common link? Neuropharmacology 2015; 97: 18–34.

Boison D, Scheurer L, Zumsteg V, Rulicke T, Litynski P, Fowler B, et al. Neonatal hepatic steatosis by disruption of the adenosine kinase gene. Proc Natl Acad Sci USA 2002; 99: 6985–90.

Boison D, Singer P, Shen HY, Feldon J, Yee BK. Adenosine hypothesis of schizophrenia–opportunities for pharmacotherapy. Neuropharmacology 2012; 62: 1527–43.

Bolon B. Pathology of the developing mouse: a systematic approach. Boca Raton: CRC Press, Taylor & Francis Group; 2015.

Burda JE, Bernstein AM, Sofroniew MV. Astrocyte roles in traumatic brain injury. Exp Neurol 2016; 275: 305–15.

Caplan HW, Cox CS, Bedi SS. Do microglia play a role in sex differences in TBI? J Neurosci Res 2017; 95: 509–17.

Chen Y, Mao H, Yang KH, Abel T, Meaney DF. A modified controlled cortical impact technique to model mild traumatic brain injury mechanics in mice. Front Neurol 2014; 5: 100.

Cole JT, Yarnell A, Kean WS, Gold E, Lewis B, Ren M, et al. Craniotomy: true sham for traumatic brain injury, or a sham of a sham? J Neurotrauma 2011; 28: 359–69.

Costello EJ, Mustillo S, Erkanli A, Keeler G, Angold A. Prevalence and development of psychiatric disorders in childhood and adolescence. Arch Gen Psychiatry 2003; 60: 837–44.

Crews FT, Mdzinarishvili A, Kim D, He J, Nixon K. Neurogenesis in adolescent brain is potently inhibited by ethanol. Neuroscience 2006; 137: 437–45.

Cui XA, Singh B, Park J, Gupta RS. Subcellular localization of adenosine kinase in mammalian cells: The long isoform of AdK is localized in the nucleus. Biochem Biophys Res Commun 2009; 388: 46–50.

Dash PK, Mach SA, Moore AN. Enhanced neurogenesis in the rodent hippocampus following traumatic brain injury. J Neurosci Res 2001; 63: 313–19.

Dong S, Dt E, Andrew R, Michael W, Robert H. Inhibition of injury-induced cell proliferation in the dentate gyrus of the hippocampus impairs spontaneous cognitive recovery after traumatic brain injury. J Neurotrauma 2015; 32: 495–505.

Dudek FE, Sutula TP. Epileptogenesis in the dentate gyrus: a critical perspective. Prog Brain Res 2007; 163: 755–73.

Fedele DE, Koch P, Brüstle O, Scheurer L, Simpson EM, Mohler H, et al. Engineering embryonic stem cell derived glia for adenosine delivery. Neurosci Lett 2004; 370: 160–5.

Gao WM, Chadha MS, Kline AE, Clark RS, Kochanek PM, Dixon CE, et al. Immunohistochemical analysis of histone H3 acetylation and methylation–evidence for altered epigenetic signaling following traumatic brain injury in immature rats. Brain Res 2006; 1070: 31–4.

Gao X, Enikolopov G, Chen J. Moderate traumatic brain injury promotes proliferation of quiescent neural progenitors in the adult hippocampus. Exp Neurol 2009; 219: 516–23.

Goncalves JT, Schafer ST, Gage FH. Adult neurogenesis in the hippocampus: from stem cells to behavior. Cell 2016; 167: 897–914.

Gouder N, Scheurer L, Fritschy JM, Boison D. Overexpression of adenosine kinase in epileptic hippocampus contributes to epileptogenesis. J Neurosci 2004; 24: 692–701.

Griesbach GS, Hovda DA, Molteni R, Gomez-Pinilla F. Alterations in BDNF and synapsin I within the occipital cortex and hippocampus after mild traumatic brain injury in the developing rat: reflections of injury-induced neuroplasticity. J Neurotrauma 2002; 19: 803–14.

Hattiangady B, Rao MS, Shetty AK. Grafting of striatal precursor cells into hippocampus shortly after status epilepticus restrains chronic temporal lobe epilepsy. Exp Neurol 2008; 212: 468–81.

Hirabayashi K, Shiota K, Yagi S. DNA methylation profile dynamics of tissue-dependent and differentially methylated regions during mouse brain development. BMC Genomics 2013; 14: 82.

Hsieh J, Zhao X. Genetics and epigenetics in adult neurogenesis. Cold Spring Harb Perspect Biol 2016; 8: a018911.

Huber A, Güttinger M, Möhler H, Boison D. Seizure suppression by adenosine A2A receptor activation in a rat model of audiogenic brainstem epilepsy. Neurosci Lett 2002; 329: 289–92.

Kernie SG, Parent JM. Forebrain neurogenesis after focal Ischemic and traumatic brain injury. Neurobiol Dis 2010; 37: 267–74.

Kiese K, Jablonski J, Boison D, Kobow K. Dynamic regulation of the adenosine kinase gene during early postnatal brain development and maturation. Front Mol Neurosci 2016; 9: 99.

Lagraoui M, Latoche JR, Cartwright NG, Sukumar G, Dalgard CL, Schaefer BC. Controlled cortical impact and craniotomy induce strikingly similar profiles of inflammatory gene expression, but with distinct kinetics. Front Neur 2012; 3: 155.

Li T, Ren G, Kaplan DL, Boison D. Human mesenchymal stem cell grafts engineered to release adenosine reduce chronic seizures in a mouse model of CA3-selective epileptogenesis. Epilepsy Res 2009; 84: 238–41.

Long Q, Upadhya D, Hattiangady B, Kim D-K, An SY, Shuai B, et al. Intranasal MSC-derived A1-exosomes ease inflammation, and prevent abnormal neurogenesis and memory dysfunction after status epilepticus. Proc Natl Acad Sci USA 2017; 201703920.

Ma DK, Jang MH, Guo JU, Kitabatake Y, Chang ML, Pow-Anpongkul N, et al. Neuronal activity-induced Gadd45b promotes epigenetic DNA demethylation and adult neurogenesis. Science 2009; 323: 1074–7.

Masino SA, Kawamura M, Jr., Cote JL, Williams RB, Ruskin DN. Adenosine and autism: a spectrum of opportunities. Neuropharmacology 2013; 68: 116–21.

McGeer PL, Schwab C, Parent A, Doudet D. Presence of reactive microglia in monkey substantia nigra years after 1-methyl-4-phenyl-1,2,3,4-tetrahydropyridine administration. Ann Neurol 2003; 54: 599–604.

Miao Z, He Y, Xin N, Sun M, Chen L, Lin L, et al. Altering 5-hydroxymethylcytosine modification impacts ischemic brain injury. Hum Mol Genet 2015; 24: 5855–66.

Neuberger EJ, Swietek B, Corrubia L, Prasanna A, Santhakumar V. Enhanced dentate neurogenesis after brain injury undermines long-term neurogenic potential and promotes seizure susceptibility. Stem Cell Rep 2017; 9: 972–84.

Osborne DM, Sandau US, Jones AT, Vander Velden JW, Weingarten AM, Etesami N, et al. Developmental role of adenosine kinase for the expression of sex-dependent neuropsychiatric behavior. Neuropharmacology 2018; 141: 89–97.

Parent JM. Adult neurogenesis in the intact and epileptic dentate gyrus. Prog Brain Res 2007; 163: 529–40.

Romine J, Gao X, Chen J. Controlled cortical impact model for traumatic brain injury. JoVE 2014; 51781.

Sandau US, Colino-Oliveira M, Jones A, Saleumvong B, Coffman SQ, Liu L, et al. Adenosine kinase deficiency in the brain results in maladaptive synaptic plasticity. J Neurosci 2016; 36: 12117–28.

Sandau US, Yahya M, Bigej R, Friedman JL, Saleumvong B, Boison D. Transient use of a systemic adenosine kinase inhibitor attenuates epilepsy development in mice. Epilepsia 2019; 60: 615–25.

Schweizer C, Balsiger S, Bluethmann H, Mansuy IM, Fritschy JM, Mohler H, et al. The gamma 2 subunit of GABA(A) receptors is required for maintenance of receptors at mature synapses. Mol Cell Neurosci 2003; 24: 442–50.

Shen HY, Singer P, Lytle N, Wei CJ, Lan JQ, Williams-Karnesky RL, et al. Adenosine augmentation ameliorates psychotic and cognitive endophenotypes of schizophrenia. J Clin Invest 2012; 122: 2567–77.

Staufner C, Lindner M, Dionisi-Vici C, Freisinger P, Dobbelaere D, Douillard C, et al. Adenosine kinase deficiency: expanding the clinical spectrum and evaluating therapeutic options. J Inherit Metab Dis 2016; 39: 273–83.

Studer FE, Fedele DE, Marowsky A, Schwerdel C, Wernli K, Vogt K, et al. Shift of adenosine kinase expression from neurons to astrocytes during postnatal development suggests dual functionality of the enzyme. Neuroscience 2006; 142: 125–37.

Toda T, Parylak SL, Linker SB, Gage FH. The role of adult hippocampal neurogenesis in brain health and disease. Mol Psychiatry 2019; 24: 67–87.

Williams-Karnesky RL, Sandau US, Lusardi TA, Lytle NK, Farrell JM, Pritchard EM, et al. Epigenetic changes induced by adenosine augmentation therapy prevent epileptogenesis. The. J Clin Invest 2013; 123: 3552–63.